Revisit to the theoretical analysis of a classical piezoelectric cantilever energy harvester

Maoying Zhou[1] Yuhong Zhao[2]

[1] Hangzhou Dianzi University
[2] Zhejiang University

December 6, 2019

Abstract

In this paper, we investigate the classical problem for a piezoelectric cantilever energy harvester. Theoretical solution to the problem is derived and compared to the solution by other authors. Asymptotic expansions of the solution is explored in the hope of finding a plausible approximation of the problem. Dependence of the output measures upon electromechanical coupling factor is therefore studies. Some advice are provided for the design of piezoelectric energy harvester.

1 Outline of the paper

The outline of the paper should be as follows:

- To obtain the closed form solution of the CPEH problem using the harmonic balance method
- Analyze the dependence of relative displacement function $u(z;\delta)$
- Tackling the dependence of output index χ_p and output measures $\tilde{V}_p$, $\tilde{I}_p$, and $\tilde{P}_p$ upon the electromechanical coupling factor δ and base excitation frequency f_b
- Derive the asymptotic expansion of the CPEH problem for the displacement function $u(z;\delta)$ and the output index χ_p
- Explore the approximation error of the asymptotic expansion and provide some clues to improve the performance

2 Introduction

The soaring development of wireless sensor networks (WSNs) and Internet of Things (IoTs) in the past decades has intrigued the research into sustainable and renewable energy sources for low-power electronics. The primary research goal is to partially or even fully replace currently used battery power or utility wall power, which are generally expensive, inconvenient, and sometimes impossible. To this end, much attention has been paid to energy harvesters, which convert the available energy in the ambient environment into usable electricity. A number of principles, mechanisms, and implementations of energy harvesters have been put forward since their first appearance in the 1990s, [1, 2, 3, 4] among which piezoelectric vibration energy harvesters (PVEHs) have gained the most widespread research popularity.

PVEHs are typically composite structures made up of some piezoelectric elements and vibration transduction mechanisms. They are generally attached to the host structures and undergo forced vibration. With the help of the vibration transduction mechanisms, the piezoelectric elements are excited in the desired vibration modes and generate electrical outputs due to direct piezoelectric effect. A majority of PVEHs work in resonance, in the sense that the maximum output power for an externally connected pure resistance is achieved when the base excitation frequency matches that of the PVEH. [5] To understand the operation principles and guide the performance optimization, researchers have proposed different mathematical models for PVEHs.

A most direct and simple approach is to use the single-degree-of-freedom (SDOF) approximation, in which the electrical domain and the mechanical domain are using SDOF resonator models respectively. Besides, the electromechanical coupling between these two domains is represented by a constant coefficient. [5, 6] This lumped-parameter model provides fruitful insights into the mechanism and dynamics behind the energy harvesting process and has been employed in the performance improvement and optimization of PVEHs. [7, 8] However, it has been shown that this model only applies to one vibration mode and exhibits considerable inaccuracy in some circumstances. [9]

A different yet improved approach is to resort to the Rayleigh-Ritz method. In this approach, electromechanical model of the PVEHs in the variational form is established based on the generalized Hamilton's principle, [10] which is then discretized to a finite-dimension matrix-form state space model using the Rayleigh-Ritz method. [11] This approach can easily be modified to admit finite element analysis and be appropriate for numerical computation. Although experimentally validated and theoretically refined, [12, 13, 14, 15] this kind of method does not reflect the resonance phenomenon and the related modal expansions.

To address the issues, a formal expansion method is developed based on the theory of functional analysis. [16] Mechanical part of the PVEH is modeled using a partial differential equation with the help of Euler-Bernoulli assumptions, while the electrical part is described with an ordinary differential equation provided that a pure resistive load is connected to the PVEH. [17] Using the eigenfunctions of a cantilever beam as the basis functions, the derived system of equations is formally expanded to obtain an infinite series of sub-systems of ordinary differential equations. This method has been validated and successfully applied to PVEHs with end mass [18], to optimize the electrode coverage [19] and some other circumstances. However, it includes infinite terms of expansion and inevitably suffers from the truncation error during numerical calculation. Besides, the basis functions adopted in the above method do not take into account the piezoelectric effect and therefore fails to capture the accurate mode shape of the PVEH theoretically.

Here in this contribution, we focus on an exact analytical model classical PVEHs. Based on the Euler-Bernoulli beam model and the linear piezoelectric relations, electromechanical model of the energy harvester is established, and then converted to a boundary value problem of ordinary differential equations using the harmonic balance method. Closed-form solution of the relative displacement function of the cantilever beam as well as the output performance measures is analyzed and numerically investigated. Asymptotic expansions of the relative displacement function are calculated to obtain approximate expressions for the output index and the related output performance measures. Tips are then provided in terms of the structure design and performance optimization of piezoelectric energy harvesters.

3 Mathematical model for a typical PVEH

As shown in Figure 1, a typical PVEH is composed of a piezoelectric composite cantilever beam attached to a host structure. For the sake of simplicity, a pure resistor is generally connected to the piezoelectric elements to represent practical electrical loads. Actually, this is a little bit of an oversimplification in the sense that no external capcitors and inductors are included in the system and that extra interface circuits and power management circuits are usually needed to achieve a better energy harvesting performance. [20, 21, 22]

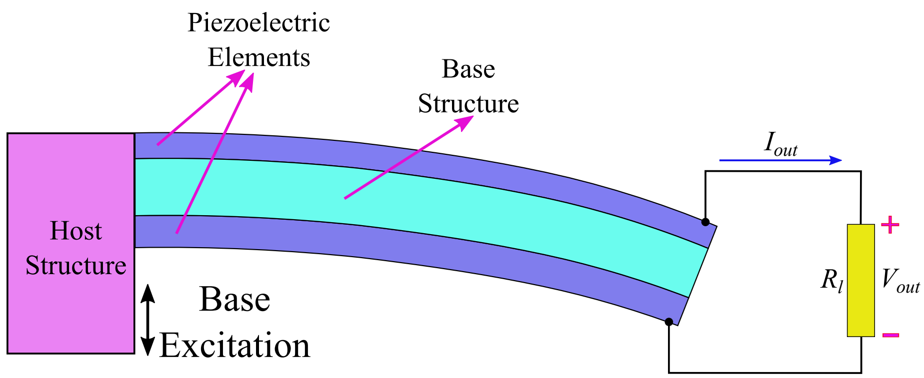

Figure 1: Schematic diagram of a typical PVEH. The bimorph structure of the PVEH is just for demonstration. Actually, many different configurations can be adopted.

Based on the Euler-Bernoulli assumptions, mechanical response of the piezoelectric composite beam is described by the classical equations

$$B_p \frac{\partial^4 w(x,t)}{\partial x^4} + m_p \frac{\partial^2 w(x,t)}{\partial t^2} = 0, \tag{1}$$

where $w(x,t)$ denotes the displacement function of the composite beam, B_p is the equivalent bending stiffness and m_p is the line mass density of the piezoelectric cantilever beam. If the piezoelectric elements attached to the cantilever beam is connected to an external electrical load R_l, we have

$$\frac{dQ_p(t)}{dt} + \frac{V_p(t)}{R_l} = 0, \tag{2}$$

in which $Q_p(t)$ is the accumulated charge on the electrodes, and $V_p(t)$ is the voltage output across the load resistor R_l. Deriving from the classic piezoelectric constitutive relations, we have

$$\begin{cases} M_p(x,t) = B_p \dfrac{\partial^2 w(x,t)}{\partial x^2} - e_p V_p(t), \\ Q_p(x,t) = e_p \left[\dfrac{\partial w(x,t)}{\partial x}\right]\Bigg|_0^{l_p} + C_p V_p(t), \end{cases} \tag{3}$$

where e_p is the piezoelectric coupling coefficient, C_p is the equivalent internal capacitance of the piezoelectric elements, and l_p is the length of the composite beam. As one end of the cantilever beam is attached to the host structure and subject to base excitation. The boundary conditions for the problems are

$$\begin{cases} w(0,t) = w_b(t), \\ \dfrac{\partial w(0,t)}{\partial x} = 0, \end{cases} \tag{4}$$

and

$$\begin{cases} M_p(l_p,t) = B_p \dfrac{\partial^2 w(l_p,t)}{\partial x^2} - e_p V_p(t) = 0, \\ N_p(l_p,t) = \dfrac{\partial M_p(l_p,t)}{\partial x} = B_p \dfrac{\partial^3 w(l_p,t)}{\partial x^3} = 0, \end{cases} \tag{5}$$

where $w_b(t)$ is the base excitation displacement, M_p and N_p are the total moment and shear force in the cross section respectively. To make things simpler, the displacement function $w(x,t)$ is be decomposed as

$$w(x,t) = w_b(t) + w_{rel}(x,t), \tag{6}$$

where $w_{rel}(x,t)$ is the relative displacement function of the composite beam. We are principally interested in a sinusoidal base excitation $w_b(t)$ which is given by

$$w_b(t) = \eta_b e^{j\sigma_b t} \tag{7}$$

where η_b is the amplitude of base excitation, and $\sigma_b = 2\pi f_b$ is the angular frequency of base excitation with f_b being the base excitation frequency. Here we use a simplified version of complex representation of a periodical signal. The term $e^{j\sigma_b t}$ should actually be $Re\left\{e^{j\sigma_b t}\right\}$. Nevertheless, this won't cause any problem in the following text and serves to simplify the calculation process. It should be noted that the amplitude η_b is generally a real number as we assume the base excitation always possesses zero phase angle.

Considering the steady state response of the PVEH to base excitation $w_b(t)$, the relative displacement function $w_{rel}(x,t)$ and output voltage $V_p(t)$ can then reasonably be represented as

$$w_{rel}(x,t) = \eta_{rel}(x) e^{j\sigma_b t}, \quad V_p(t) = \tilde{V}_p e^{j\sigma_b t}, \tag{8}$$

respectively, where $\eta_{rel}(x)$ and $\tilde{V}_p$ are complex amplitudes. In this way, the above model for the PVEH is simplified as

$$B_p \frac{\partial^4 \eta_{rel}(x)}{\partial x^4} - m_p \sigma_b^2 \eta_{rel}(x) = m_p \sigma_b^2 \eta_b, \tag{9a}$$

$$\eta_{rel}(0) = 0, \tag{9b}$$

$$\frac{\partial \eta_{rel}(0)}{\partial x} = 0, \tag{9c}$$

$$B_p \frac{\partial^2 \eta_{rel}(l_p)}{\partial x^2} + \frac{j\sigma_b R_l}{1 + j\sigma_b C_p R_l} e_p^2 \frac{\partial \eta_{rel}(l_p)}{\partial x} = 0, \tag{9d}$$

$$\frac{\partial^3 \eta_{rel}(l_p)}{\partial x^3} = 0. \tag{9e}$$

Here some discussions are to be made. Due to the existence of piezoelectric effect, the boundary conditions (9d) is tuned and deviates from the case of a pure elastic cantilever beam. [23] Hence for the related free vibration problem, the eigenvalue and eigenfunctions are different from that of a pure elastic cantilever beam, which is adopted in the work by Erturk and Inman [17, 18]. Therefore the method used by Erturk and Inman [17, 18] to expand the relative displacement function $\eta_{rel}(x)$ in terms of the eigenfunctions for a pure elastic cantilever beam is a formal one in the sense that the boundary conditions are not fulfilled by the eigenfunctions. Nonetheless, due to the orthogonality of the eigenfunctions, the expansion is mathematically feasible and a considerable accuracy can be achieved when the number of terms of expansion is large enough. This is not a perfect solution. We would like in the following to derive an exact solution to the steady state response.

To enhance the universality of our solution, we adopt the following dimensionless scheme

$$u = \eta_{rel}/\eta_b, \quad z = x/l_p \tag{10}$$

and therefore obtain the following dimensionless parameters

$$\sigma = \sigma_b \sqrt{\frac{m_p l_p^4}{B_p}}, \quad \beta = R_l C_p \sqrt{\frac{B_p}{m_p l_p^4}}, \quad \delta = \frac{e_p^2 l_p}{C_p B_p}. \tag{11}$$

Now, the above problem is converted into the following system of boundary value problem

$$\begin{cases} u'''' - \sigma^2 u = \sigma^2, \\ u(0) = 0, \\ u'(0) = 0, \\ u''(1) + \dfrac{j\beta\sigma}{1 + j\beta\sigma} \delta u'(1) = 0, \\ u'''(1) = 0, \end{cases} \tag{12}$$

where the prime denotes the derivative with respect to z.

4 Theoretical analysis of the model

The boundary value problem (12) is a linear problem depending on the three dimensionless parameters β, σ, and δ. Due to the presence of complex tuning terms in the boundary conditions, the solution $u(z)$ is generically a complex function. The analytical solution to this problem can be formulated as

$$u(z;\delta) = A_\delta \cos\sqrt{\sigma} z + B_\delta \sin\sqrt{\sigma} z + C_\delta \cosh\sqrt{\sigma} z + D_\delta \sinh\sqrt{\sigma} z - 1. \tag{13}$$

Here we use the notation $u(z;\delta)$ to emphasize the dependence of the function $u(z)$ upon parameter δ. In the following text, we will frequently use these two notations interchangeably unless otherwise declared. The coefficients A_δ, B_δ, C_δ, and D_δ are then subject to the following linear system of equations:

$$\begin{cases} A_\delta + C_\delta = 1, \\ B_\delta + D_\delta = 0, \\ \left(-A_\delta \cos\sqrt{\sigma} - B_\delta \sin\sqrt{\sigma} + C_\delta \cosh\sqrt{\sigma} + D_\delta \sinh\sqrt{\sigma}\right) + \\ \dfrac{j\beta\sqrt{\sigma}}{j\sigma\beta + 1} \delta \left(-A_\delta \sin\sqrt{\sigma} + B_\delta \cos\sqrt{\sigma} + C_\delta \sinh\sqrt{\sigma} + D_\delta \cosh\sqrt{\sigma}\right) = 0, \\ A_\delta \sin\sqrt{\sigma} - B_\delta \cos\sqrt{\sigma} + C_\delta \sinh\sqrt{\sigma} + D_\delta \cosh\sqrt{\sigma} = 0. \end{cases} \tag{14}$$

Analytically, we can directly obtain the solution to this problem as

$$\begin{cases} A_\delta = \dfrac{1+\cos\sqrt{\sigma}\cosh\sqrt{\sigma}-\sin\sqrt{\sigma}\sinh\sqrt{\sigma}+\frac{2j\beta\sqrt{\sigma}}{1+j\beta\sigma}\delta\left(\cos\sqrt{\sigma}\sinh\sqrt{\sigma}\right)}{2\left[1+\cos\sqrt{\sigma}\cosh\sqrt{\sigma}+\frac{j\beta\sqrt{\sigma}}{1+j\beta\sigma}\delta\left(\cos\sqrt{\sigma}\sinh\sqrt{\sigma}+\sin\sqrt{\sigma}\cosh\sqrt{\sigma}\right)\right]}, \\ B_\delta = \dfrac{\cos\sqrt{\sigma}\sinh\sqrt{\sigma}+\sin\sqrt{\sigma}\cosh\sqrt{\sigma}+\frac{2j\beta\sqrt{\sigma}}{1+j\beta\sigma}\delta\left(\sin\sqrt{\sigma}\sinh\sqrt{\sigma}\right)}{2\left[1+\cos\sqrt{\sigma}\cosh\sqrt{\sigma}+\frac{j\beta\sqrt{\sigma}}{1+j\beta\sigma}\delta\left(\cos\sqrt{\sigma}\sinh\sqrt{\sigma}+\sin\sqrt{\sigma}\cosh\sqrt{\sigma}\right)\right]}, \\ C_\delta = \dfrac{1+\cos\sqrt{\sigma}\cosh\sqrt{\sigma}+\sin\sqrt{\sigma}\sinh\sqrt{\sigma}+\frac{2j\beta\sqrt{\sigma}}{1+j\beta\sigma}\delta\left(\sin\sqrt{\sigma}\cosh\sqrt{\sigma}\right)}{2\left[1+\cos\sqrt{\sigma}\cosh\sqrt{\sigma}+\frac{j\beta\sqrt{\sigma}}{1+j\beta\sigma}\delta\left(\cos\sqrt{\sigma}\sinh\sqrt{\sigma}+\sin\sqrt{\sigma}\cosh\sqrt{\sigma}\right)\right]}, \\ D_\delta = \dfrac{-\cos\sqrt{\sigma}\sinh\sqrt{\sigma}-\sin\sqrt{\sigma}\cosh\sqrt{\sigma}-\frac{2j\beta\sqrt{\sigma}}{1+j\beta\sigma}\delta\left(\sin\sqrt{\sigma}\sinh\sqrt{\sigma}\right)}{2\left[1+\cos\sqrt{\sigma}\cosh\sqrt{\sigma}+\frac{j\beta\sqrt{\sigma}}{1+j\beta\sigma}\delta\left(\cos\sqrt{\sigma}\sinh\sqrt{\sigma}+\sin\sqrt{\sigma}\cosh\sqrt{\sigma}\right)\right]}. \end{cases} \tag{15}$$

Equations (13) and (15) suffice to determine the analytical solution to the problem (12). To validate this form of solution expressions for $u(z;\delta)$, we use the physical and mechanical parameters shown in [17] and calculate the dimensionless relative displacement function $u(z;\delta)$ and the corresponding normalized output voltage $|\tilde{V}_p/(\sigma_b^2\eta_b)|$ at different base excitation frequency f_b and load resistance R_l. The results are presented in Figure 2, where Figure 2(a) contains the results calculated by our method and Figure 2(b) is adapted from the reference [17]. It is seen that the two sets of results are close to each other, especially at small values of f_b. No obvious difference is present for the resonant frequency of the first order resonant mode. However the calculated resonant frequency for higher order resonant mode is clearly different. The third order resonant frequency is smaller than 800 Hz in our model but larger than 800 Hz in the model by Erturk and Inman [17]. Besides, the behaviors of the two solutions are different around the resonance. Our model predict a sharper peak. This could explained as follows. In the numerical calculations of our model, the grid steps for frequency can be chosen to be as small as possible. A finer calculation grid leads to a sharper resonant peak. Besides, the calculation of the model by Erturk and Inman [17] always involves with the truncation of the infinite expansion into finite terms, which introduces considerable error for larger values of f_b, especially at resonance.

After validation, we are interested in the influence of parameter value δ upon the resulting dimensionless relative displacement function $u(z;\delta)$. According to equations (13) and (15), the dimensionless relative displacement function $u(z;\delta)$ is completely determined by the three dimensionless parameters σ, β, and δ. which can be interpreted as the dimensionless base excitation frequency, the dimensionless electrical resonant frequency, and the dimensionless electromechanical coupling strength for the PVEH respectively. As σ and β is determined by the base excitation f_b and externally connected load R_l respectively, only the parameter δ is fully determined by the structure itself. By taking different values of δ , we calculate the dimensionless relative displacement function $u(z;\delta)$ and plot the results in Figure 3.

It is shown in Figure 3 that the parameter δ changes the function $u(z;\delta)$ through the change of the third boundary condition in the system (12). When δ is zero, i.e., no electromechanical coupling is present, the system degenerates to the classical elastic cantilever beam problem, whose solution is a real function. That is to say, the phase of $u(z;\delta)$ is constantly zero across the whole beam (in the range of $0 \le z \le 1$). Analytical expressions for the coefficients in this case are

$$\begin{cases} A_\varnothing = \dfrac{1+\cos\sqrt{\sigma}\cosh\sqrt{\sigma}-\sin\sqrt{\sigma}\sinh\sqrt{\sigma}}{2\left[1+\cos\sqrt{\sigma}\cosh\sqrt{\sigma}\right]}, \\ B_\varnothing = \dfrac{\cos\sqrt{\sigma}\sinh\sqrt{\sigma}+\sin\sqrt{\sigma}\cosh\sqrt{\sigma}}{2\left[1+\cos\sqrt{\sigma}\cosh\sqrt{\sigma}\right]}, \\ C_\varnothing = \dfrac{1+\cos\sqrt{\sigma}\cosh\sqrt{\sigma}+\sin\sqrt{\sigma}\sinh\sqrt{\sigma}}{2\left[1+\cos\sqrt{\sigma}\cosh\sqrt{\sigma}\right]}, \\ D_\varnothing = \dfrac{-\cos\sqrt{\sigma}\sinh\sqrt{\sigma}-\sin\sqrt{\sigma}\cosh\sqrt{\sigma}}{2\left[1+\cos\sqrt{\sigma}\cosh\sqrt{\sigma}\right]}, \end{cases} \tag{16}$$

and the resultant dimensionless relative displacement function $u_\varnothing(z)$ is represented as

$$u_\varnothing(z) = A_\varnothing\cos\sqrt{\sigma}z + B_\varnothing\sin\sqrt{\sigma}z + C_\varnothing\cosh\sqrt{\sigma}z + D_\varnothing\sinh\sqrt{\sigma}z - 1. \tag{17}$$

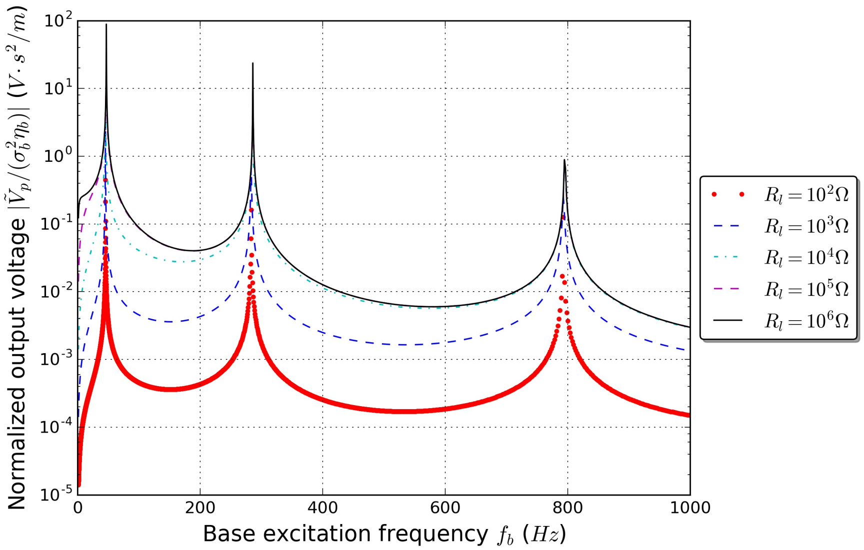

(a)

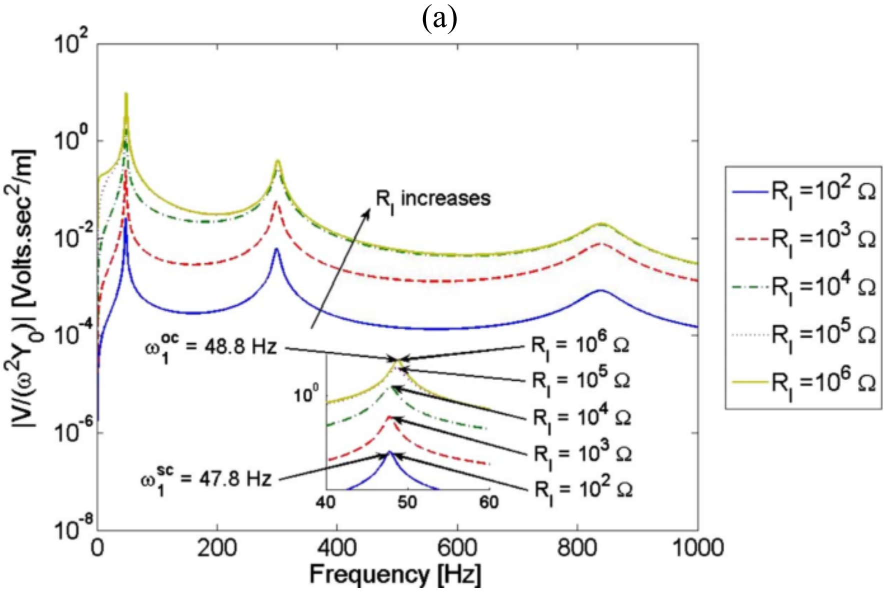

(b)

Figure 2: Comparison of the currently obtained results (a) with that (b) by Erturk and Inman [17].

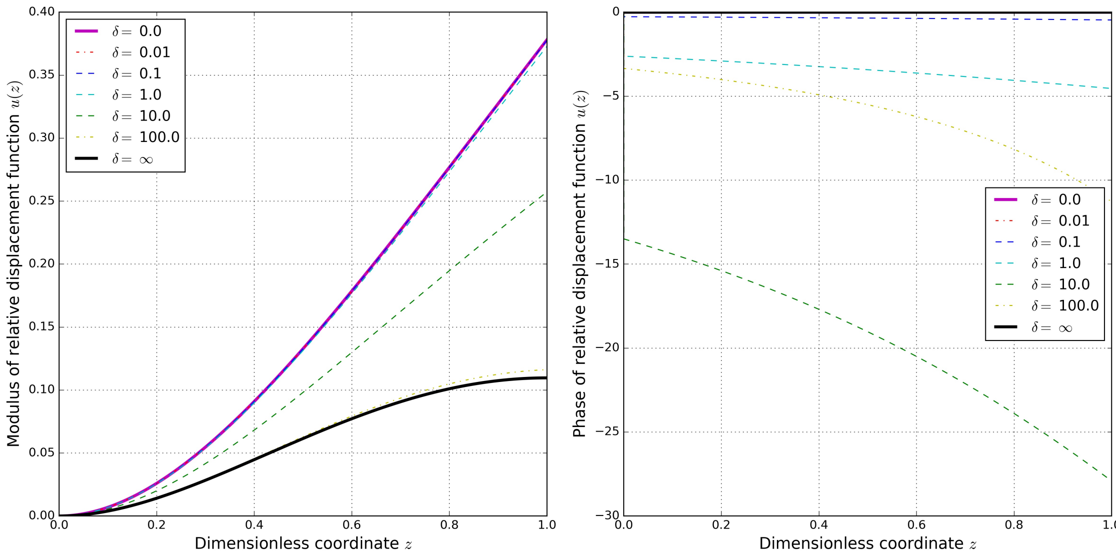

Figure 3: Modulus (left panel) and phase (left panel) of the displacement function $u(z;\delta)$ for different values of δ. Note that for the case of $\delta = 0$ and $\delta = \infty$, the phase is always zero and hence invisible in the figure. The results are calculated at the parameter value of $\beta = 0.064$ and $\sigma = 1.557$.

When the electromechanical coupling is extremely strong, δ is extremely large and can be seen as ∞ in mathematical sense. In this situation, the solution $u_\infty(z)$ is again real without any phase difference in the z direction. The coefficients can be analytically expressed as

$$\begin{cases} A_\infty = \dfrac{\cos\sqrt{\sigma}\sinh\sqrt{\sigma}}{\cos\sqrt{\sigma}\sinh\sqrt{\sigma}+\sin\sqrt{\sigma}\cosh\sqrt{\sigma}}, \\ B_\infty = \dfrac{\sin\sqrt{\sigma}\sinh\sqrt{\sigma}}{\cos\sqrt{\sigma}\sinh\sqrt{\sigma}+\sin\sqrt{\sigma}\cosh\sqrt{\sigma}}, \\ C_\infty = \dfrac{\sin\sqrt{\sigma}\cosh\sqrt{\sigma}}{\cos\sqrt{\sigma}\sinh\sqrt{\sigma}+\sin\sqrt{\sigma}\cosh\sqrt{\sigma}}, \\ D_\infty = \dfrac{-\sin\sqrt{\sigma}\sinh\sqrt{\sigma}}{\cos\sqrt{\sigma}\sinh\sqrt{\sigma}+\sin\sqrt{\sigma}\cosh\sqrt{\sigma}}, \end{cases} \tag{18}$$

and hence the dimensionless relative displacement function $u_\infty(z)$ is

$$u_\infty(z) = A_\infty\cos\sqrt{\sigma}z + B_\infty\sin\sqrt{\sigma}z + C_\infty\cosh\sqrt{\sigma}z + D_\infty\sinh\sqrt{\sigma}z - 1. \tag{19}$$

While a finite non-zero electromechanical coupling factor δ is present, as expected in most applications, modulus and phase of the dimensionless displacement function $u(z;\delta)$ are both changing along the z direction. Nevertheless, it is seen from the right panel of Figure 3 that when the values of δ is either small or large, the phase change of $u(z;\delta)$ is very small in the z direction. To make it more clear, we plot the modulus and phase of $u(z;\delta)$ at $z = 1$ versus different values of δ in Figure 4. It is clear that with the increase of δ, modulus of $u(1;\delta)$ decreases, while its phase reaches a minimum at some intermediate value of δ (Here around $\delta = 20$). This also explains the fact expressed in Figure 3 that the modulus of dimensionless relative displacement function $u_\delta(z)$ with $0 < \delta < \infty$ is always between that of $u_\varnothing(z)$ and $u_\infty(z)$.

As for the output voltage $V_p(t)$, output current $I_p(t)$, and output power $P_p(t)$ of the PVEH, the corresponding complex amplitudes $\tilde{V}_p$, $\tilde{I}_p$, and $\tilde{P}_p$ can be formulated as

$$\begin{cases} \tilde{V}_p = -\dfrac{j\sigma\beta}{j\sigma\beta+1}\dfrac{\eta_b}{l_p}\dfrac{e_p}{C_p}u'(1) = -\dfrac{j\sigma\beta}{j\sigma\beta+1}\dfrac{\eta_b}{l_p}\dfrac{e_p}{C_p}\chi_p, \\ \tilde{I}_p = \tilde{V}_p/R_l = -\dfrac{j\sigma\beta}{j\sigma\beta+1}\left(\dfrac{\eta_b}{l_p}\right)\left(\dfrac{e_p}{C_pR_l}\right)\chi_p, \\ \tilde{P}_p = \tilde{V}_p^2/R_l = \left(\dfrac{\eta_b}{l_p}\right)^2\left(\dfrac{e_p}{C_p}\right)\left(\dfrac{e_p}{C_pR_l}\right)\left(\dfrac{j\sigma\beta}{j\sigma\beta+1}\right)^2\chi_p^2, \end{cases} \tag{20}$$

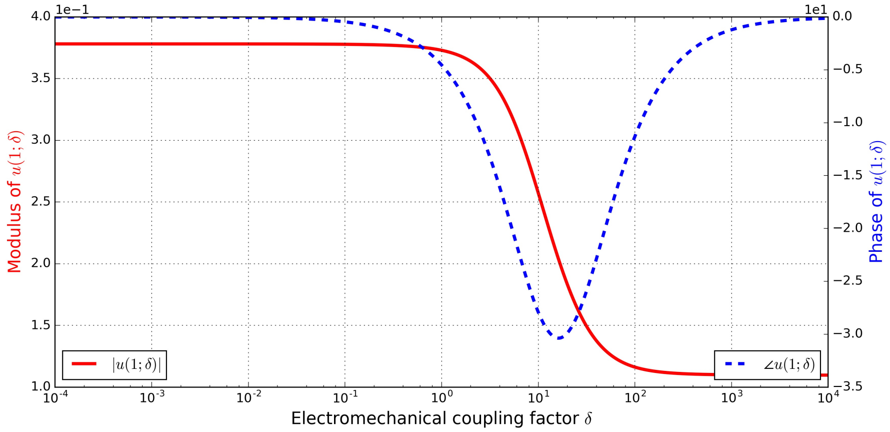

Figure 4: Modulus and phase of the displacement function $u(z;\delta)$ at the position $z = 1$ versus electromechanical coupling factor δ. The results are calculated at the parameter value of $\beta = 0.064$ and $\sigma = 1.557$.

in which we have used the notations of output index χ_p

$$\chi_p = u_1'(1) = \frac{\sqrt{\sigma}\,(\sinh\sqrt{\sigma} - \sin\sqrt{\sigma})}{1 + \cos\sqrt{\sigma}\cosh\sqrt{\sigma} + \frac{j\beta\sqrt{\sigma}}{1+j\beta\sigma}\delta\,(\cos\sqrt{\sigma}\sinh\sqrt{\sigma} + \sin\sqrt{\sigma}\cosh\sqrt{\sigma})}. \tag{21}$$

Clearly, The three output measures $\tilde{V}_p$, $\tilde{I}_p$, and $\tilde{P}_p$ are heavily dependent on another dimensionless parameter $r_d = \eta_b/l_p$, which is the dimensionless base excitation amplitude. Formally, both $\tilde{V}_p$ and $\tilde{I}_p$ depend linearly upon r_d, while $\tilde{P}_p$ shows a quadratic dependence on r_d. The only dependence upon δ is introduced in χ_p. However, it should be noted that the definition of parameter δ relies on e_p, l_p, C_p, and B_p, while the three measures $\tilde{V}_p$, $\tilde{I}_p$, and $\tilde{P}_p$ are dimensional values and depend on e_p, σ_b, and R_l. As a result, the change of parameter δ results in the change of reference voltage e_p/C_p, reference current $e_p/(C_pR_l)$, and reference power $(e_p/C_p)[e_p/(C_pR_l)]$, and therefore the corresponding values of $\tilde{V}_p$, $\tilde{I}_p$, and $\tilde{P}_p$. Hence, we may establish a bijective relation between δ and e_p, and relate the change of δ to that of e_p. In this way, we calculate the three output measures $\tilde{V}_p$, $\tilde{I}_p$, and $\tilde{P}_p$ at different values of δ and plot their moduli in Figure 5.

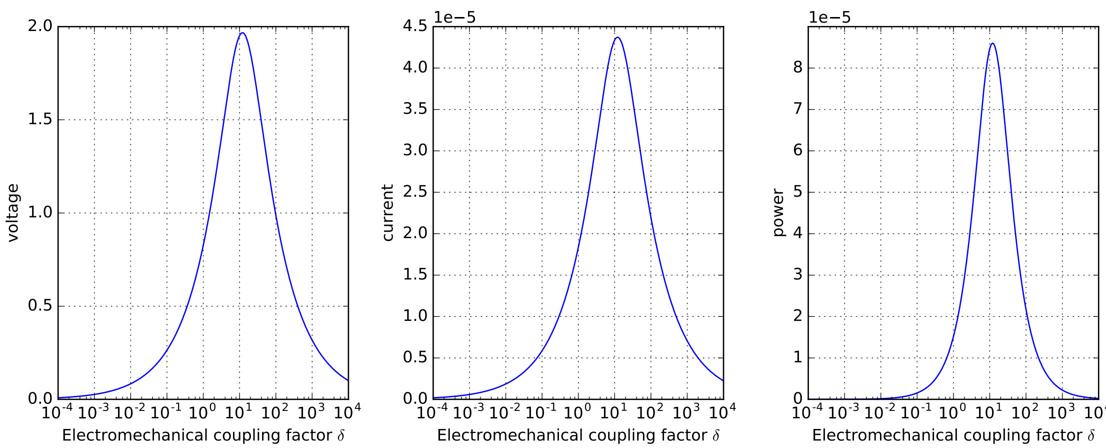

Figure 5: Voltage, current and power output for the piezoelectric cantilever energy harvester

It is seen from Figure 5 that all the three measures show a maximum peak with the increase of δ at the approximate value of $\delta = 10$. When δ is small, or equivalently, e_p is small, amplitude of the three output measures $\tilde{V}_p$, $\tilde{I}_p$, and $\tilde{P}_p$ increase with the increase of δ. Then after the critical value of δ, a further increase of δ causes the decrease of output measures. Thus we come to a small conclusion that to obtain an optimal output performance, the electromechanical coupling factor δ should be set to an appropriate value. However, a direct calculation using the parameters introduced in the literature [17, 18] shows that the parameter δ is rather small for a typical piezoelectric cantilever energy harvester. For example, for a piezoelectric voltage constant $e_{31} = -5.35\ C/m^2$, the value of e_p is $-5.35\times10^{-5}\ C$, and the final value of δ is 0.028. According to the properties of commonly used piezoelectric materials, the parameter e_{31} is always in the range of several or several tens C/m^2 reference to be inserted. That is to say, the final value of δ can be seen always in the order of 10^{-2}, which is a rather small value according to the diagram. Hence we could present an asymptotic analysis of the performance of the classical piezoelectric energy harvester. This is the subject of the following section.

5 Asymptotic analysis of the problem

Considering that the parameter δ is small, we expand the theoretical solution to the problem in terms of the small parameter δ using the following regular expansion:

$$\begin{cases} A_\delta = A_0 + \delta A_1 + \delta^2 A_2 + \cdots, \\ B_\delta = B_0 + \delta B_1 + \delta^2 B_2 + \cdots, \\ C_\delta = C_0 + \delta C_1 + \delta^2 C_2 + \cdots, \\ D_\delta = D_0 + \delta D_1 + \delta^2 D_2 + \cdots. \end{cases} \tag{22}$$

As a result, we obtain the following successive expansion problem:
$O(\delta^0)$:

$$\begin{cases} A_0 + C_0 = 1, \\ B_0 + D_0 = 0, \\ -A_0 \cos\sqrt{\sigma} - B_0 \sin\sqrt{\sigma} + C_0 \cosh\sqrt{\sigma} + D_0 \sinh\sqrt{\sigma} = 0, \\ A_0 \sin\sqrt{\sigma} - B_0 \cos\sqrt{\sigma} + C_0 \sinh\sqrt{\sigma} + D_0 \cosh\sqrt{\sigma} = 0. \end{cases} \tag{23}$$

The solution is

$$\begin{cases} A_0 = \dfrac{1 + \cos\sqrt{\sigma}\cosh\sqrt{\sigma} - \sin\sqrt{\sigma}\sinh\sqrt{\sigma}}{2 + 2\cos\sqrt{\sigma}\cosh\sqrt{\sigma}}, \\ B_0 = \dfrac{\cosh\sqrt{\sigma}\sin\sqrt{\sigma} + \cos\sqrt{\sigma}\sinh\sqrt{\sigma}}{2 + 2\cos\sqrt{\sigma}\cosh\sqrt{\sigma}}, \\ C_0 = \dfrac{1 + \cos\sqrt{\sigma}\cosh\sqrt{\sigma} + \sin\sqrt{\sigma}\sinh\sqrt{\sigma}}{2 + 2\cos\sqrt{\sigma}\cosh\sqrt{\sigma}}, \\ D_0 = -\dfrac{\cosh\sqrt{\sigma}\sin\sqrt{\sigma} + \cos\sqrt{\sigma}\sinh\sqrt{\sigma}}{2 + 2\cos\sqrt{\sigma}\cosh\sqrt{\sigma}}. \end{cases} \tag{24}$$

Hence we have

$$-A_0 \sin\sqrt{\sigma} + B_0 \cos\sqrt{\sigma} + C_0 \sinh\sqrt{\sigma} + D_0 \cosh\sqrt{\sigma} = \frac{\sinh\sqrt{\sigma} - \sin\sqrt{\sigma}}{\cos\sqrt{\sigma}\cosh\sqrt{\sigma} + 1} \tag{25}$$

$O(\delta^1)$:

$$\begin{cases} A_1 + C_1 = 0, \\ B_1 + D_1 = 0, \\ \left(-A_1 \cos\sqrt{\sigma} - B_1 \sin\sqrt{\sigma} + C_1 \cosh\sqrt{\sigma} + D_1 \sinh\sqrt{\sigma}\right) + \\ \dfrac{j\beta\sqrt{\sigma}}{j\sigma\beta + 1}\left(-A_0 \sin\sqrt{\sigma} + B_0 \cos\sqrt{\sigma} + C_0 \sinh\sqrt{\sigma} + D_0 \cosh\sqrt{\sigma}\right) = 0, \\ A_1 \sin\sqrt{\sigma} - B_1 \cos\sqrt{\sigma} + C_1 \sinh\sqrt{\sigma} + D_1 \cosh\sqrt{\sigma} = 0. \end{cases} \tag{26}$$

The solution is

$$
\begin{cases}
A_1 = \dfrac{j\beta\sqrt{\sigma}}{1+j\beta\sigma}\left(\dfrac{\sinh\sqrt{\sigma}-\sin\sqrt{\sigma}}{\cos\sqrt{\sigma}\cosh\sqrt{\sigma}+1}\right)\left(\dfrac{\cos\sqrt{\sigma}+\cosh\sqrt{\sigma}}{2\cos\sqrt{\sigma}\cosh\sqrt{\sigma}+2}\right)\\
B_1 = \dfrac{j\beta\sqrt{\sigma}}{1+j\beta\sigma}\left(\dfrac{\sinh\sqrt{\sigma}-\sin\sqrt{\sigma}}{\cos\sqrt{\sigma}\cosh\sqrt{\sigma}+1}\right)\left(\dfrac{-\sinh\sqrt{\sigma}+\sin\sqrt{\sigma}}{2\cos\sqrt{\sigma}\cosh\sqrt{\sigma}+2}\right)\\
C_1 = \dfrac{j\beta\sqrt{\sigma}}{1+j\beta\sigma}\left(\dfrac{\sinh\sqrt{\sigma}-\sin\sqrt{\sigma}}{\cos\sqrt{\sigma}\cosh\sqrt{\sigma}+1}\right)\left(-\dfrac{\cos\sqrt{\sigma}+\cosh\sqrt{\sigma}}{2\cos\sqrt{\sigma}\cosh\sqrt{\sigma}+2}\right)\\
D_1 = \dfrac{j\beta\sqrt{\sigma}}{1+j\beta\sigma}\left(\dfrac{\sinh\sqrt{\sigma}-\sin\sqrt{\sigma}}{\cos\sqrt{\sigma}\cosh\sqrt{\sigma}+1}\right)\left(\dfrac{-\sin\sqrt{\sigma}+\sinh\sqrt{\sigma}}{2\cos\sqrt{\sigma}\cosh\sqrt{\sigma}+2}\right)
\end{cases}
\tag{27}
$$

Then we have

$$
\begin{aligned}
&-A_1\sin\sqrt{\sigma}+B_1\cos\sqrt{\sigma}+C_1\sinh\sqrt{\sigma}+D_1\cosh\sqrt{\sigma}\\
&=\frac{j\beta\sqrt{\sigma}}{1+j\beta\sigma}\left(\frac{\sin\sqrt{\sigma}-\sinh\sqrt{\sigma}}{\cos\sqrt{\sigma}\cosh\sqrt{\sigma}+1}\right)\left(\frac{\cos\sqrt{\sigma}\sinh\sqrt{\sigma}+\sin\sqrt{\sigma}\cosh\sqrt{\sigma}}{\cos\sqrt{\sigma}\cosh\sqrt{\sigma}+1}\right)
\end{aligned}
\tag{28}
$$

$O(\delta^2)$:

$$
\begin{cases}
A_2 + C_2 = 0,\\
B_2 + D_2 = 0,\\
\left(-A_2\cos\sqrt{\sigma}-B_2\sin\sqrt{\sigma}+C_2\cosh\sqrt{\sigma}+D_2\sinh\sqrt{\sigma}\right)+\\
\dfrac{j\beta\sqrt{\sigma}}{j\sigma\beta+1}\left(-A_1\sin\sqrt{\sigma}+B_1\cos\sqrt{\sigma}+C_1\sinh\sqrt{\sigma}+D_1\cosh\sqrt{\sigma}\right)=0,\\
A_2\sin\sqrt{\sigma}-B_2\cos\sqrt{\sigma}+C_2\sinh\sqrt{\sigma}+D_2\cosh\sqrt{\sigma}=0.
\end{cases}
\tag{29}
$$

The solution is

$$
\begin{cases}
A_2 = \left(\dfrac{j\beta\sqrt{\sigma}}{1+j\beta\sigma}\right)^2\left(\dfrac{\sinh\sqrt{\sigma}-\sin\sqrt{\sigma}}{\cos\sqrt{\sigma}\cosh\sqrt{\sigma}+1}\right)\left(\dfrac{\cos\sqrt{\sigma}\sinh\sqrt{\sigma}+\sin\sqrt{\sigma}\cosh\sqrt{\sigma}}{\cos\sqrt{\sigma}\cosh\sqrt{\sigma}+1}\right)\left(\dfrac{\cos\sqrt{\sigma}+\cosh\sqrt{\sigma}}{2\cos\sqrt{\sigma}\cosh\sqrt{\sigma}+2}\right)\\
B_2 = \left(\dfrac{j\beta\sqrt{\sigma}}{1+j\beta\sigma}\right)^2\left(\dfrac{\sinh\sqrt{\sigma}-\sin\sqrt{\sigma}}{\cos\sqrt{\sigma}\cosh\sqrt{\sigma}+1}\right)\left(\dfrac{\cos\sqrt{\sigma}\sinh\sqrt{\sigma}+\sin\sqrt{\sigma}\cosh\sqrt{\sigma}}{\cos\sqrt{\sigma}\cosh\sqrt{\sigma}+1}\right)\left(\dfrac{-\sinh\sqrt{\sigma}+\sin\sqrt{\sigma}}{2\cos\sqrt{\sigma}\cosh\sqrt{\sigma}+2}\right)\\
C_2 = \left(\dfrac{j\beta\sqrt{\sigma}}{1+j\beta\sigma}\right)^2\left(\dfrac{\sinh\sqrt{\sigma}-\sin\sqrt{\sigma}}{\cos\sqrt{\sigma}\cosh\sqrt{\sigma}+1}\right)\left(\dfrac{\cos\sqrt{\sigma}\sinh\sqrt{\sigma}+\sin\sqrt{\sigma}\cosh\sqrt{\sigma}}{\cos\sqrt{\sigma}\cosh\sqrt{\sigma}+1}\right)\left(-\dfrac{\cos\sqrt{\sigma}+\cosh\sqrt{\sigma}}{2\cos\sqrt{\sigma}\cosh\sqrt{\sigma}+2}\right)\\
D_2 = \left(\dfrac{j\beta\sqrt{\sigma}}{1+j\beta\sigma}\right)^2\left(\dfrac{\sinh\sqrt{\sigma}-\sin\sqrt{\sigma}}{\cos\sqrt{\sigma}\cosh\sqrt{\sigma}+1}\right)\left(\dfrac{\cos\sqrt{\sigma}\sinh\sqrt{\sigma}+\sin\sqrt{\sigma}\cosh\sqrt{\sigma}}{\cos\sqrt{\sigma}\cosh\sqrt{\sigma}+1}\right)\left(\dfrac{-\sin\sqrt{\sigma}+\sinh\sqrt{\sigma}}{2\cos\sqrt{\sigma}\cosh\sqrt{\sigma}+2}\right)
\end{cases}
\tag{30}
$$

Indeed, we can continue to obtain the coefficients for higher order (≥ 2) expansions, as shown in the appendices (To add some comments) using successive iteration method. Nevertheless, it suffices here to consider up to the second order expansion $u^{(0)}(z)$, $u^{(1)}(z)$, and $u^{(2)}(z)$, respectively:

$$
\begin{cases}
u^{(0)}(z) = u_0(z),\\
u^{(1)}(z) = u_0(z) + \delta u_1(z),\\
u^{(2)}(z) = u_0(z) + \delta u_1(z) + \delta^2 u_2(z),
\end{cases}
\tag{31}
$$

where the terms $u_0(z)$, $u_1(z)$, and $u_2(z)$ are defined as

$$
\begin{cases}
u_0(z) = A_0\cos\sqrt{\sigma}z + B_0\sin\sqrt{\sigma}z + C_0\cosh\sqrt{\sigma}z + D_0\sinh\sqrt{\sigma}z - 1,\\
u_1(z) = A_1\cos\sqrt{\sigma}z + B_1\sin\sqrt{\sigma}z + C_1\cosh\sqrt{\sigma}z + D_1\sinh\sqrt{\sigma}z,\\
u_2(z) = A_2\cos\sqrt{\sigma}z + B_2\sin\sqrt{\sigma}z + C_2\cosh\sqrt{\sigma}z + D_2\sinh\sqrt{\sigma}z.
\end{cases}
\tag{32}
$$

For different values of δ and σ (Here in this simulation, the value of σ is changed through the variance of base excitation frequency f_b), the asymptotic approximations of the dimensionless relative beam displacement function $u(z;\delta)$ up to the second order $u^{(0)}(z)$, $u^{(1)}(z)$, and $u^{(2)}(z)$ are calculated and compared to the closed solution $u(z;\delta)$ itself. The results are shown in Figure 6, 7, 8, 9, 10, 11, 12.

Notice from Figure 2 that the first mode resonant frequency for the device is around 45 Hz. It is seen from these results that a smaller value of δ results in a better approximation, whatever the value of f_b. This is consistent with the philosophy behind asymptotic expansion. Besides, for the frequency away from the resonant frequency, the approximation results are relatively accurate in

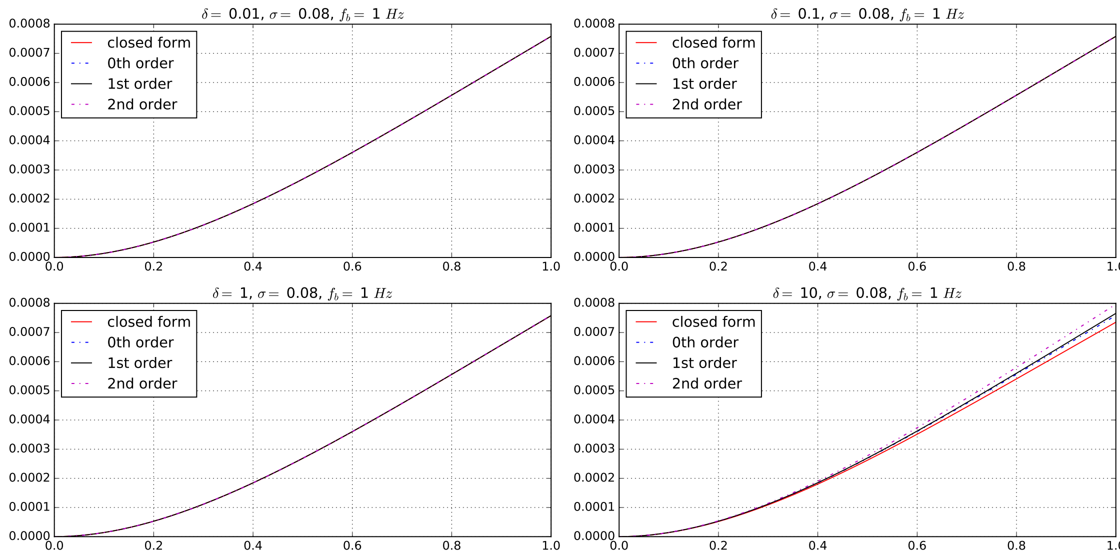

Figure 6: Comparison for the different orders of asymptotic expansion for the dimensionless relative displacement function $u_\delta(z)$.

the range of $\delta \leq 0.1$ depending on the value of f_b. While when the base excitation frequency f_b is close to a resonance, for example $f_b = 45\ Hz$, the approximation results are not accurate even at the value of $\delta = 0.01$. That is to say, the asymptotic expansion in terms of δ is not uniform with respect to parameter σ. Especially, the existence of resonance actually restrict the behavior of the asymptotic expansion. Around the resonance the expansion will show low accuracy, while away from the resonance, the expansion accuracy is easily retained. Nonetheless, for commonly used piezoelectric materials and energy harvesting device configuration, the value of δ is usually in the range of 10^{-2}. Hence, it is generally validated to use the asymptotic expansion method to approximate the dimensionless displacement function $u(z;\delta)$. Furthermore, in view of the approximating performances of the asymptotic expansions to different orders, it suffices to keep only the $0th$ order terms. Then, we have that

$$u(z;\delta) \approx u^{(0)}(z) = A_0 \cos\sqrt{\sigma}z + B_0 \sin\sqrt{\sigma}z + C_0 \cosh\sqrt{\sigma}z + D_0 \sinh\sqrt{\sigma}z - 1. \tag{33}$$

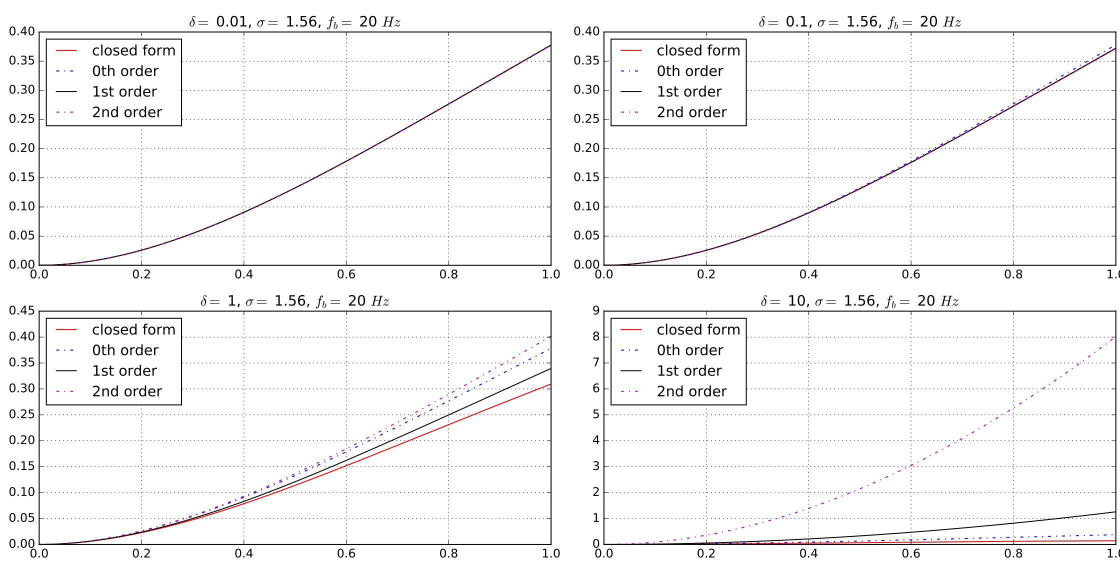

Figure 7: Comparison for the different orders of asymptotic expansion for the dimensionless relative displacement function $u_\delta(z)$.

This is exactly the displacement function of a pure elastic cantilever beam. It means that for most piezoelectric energy harvesting devices, due to the fact that the electromechanical coupling factor is relatively small, the displacement function is not much affected. In this way, we have indeed uncoupled the electrical part and elastic part of a piezoelectric energy harvesting device. It should be noted that the approximation is not valid near the resonant points.

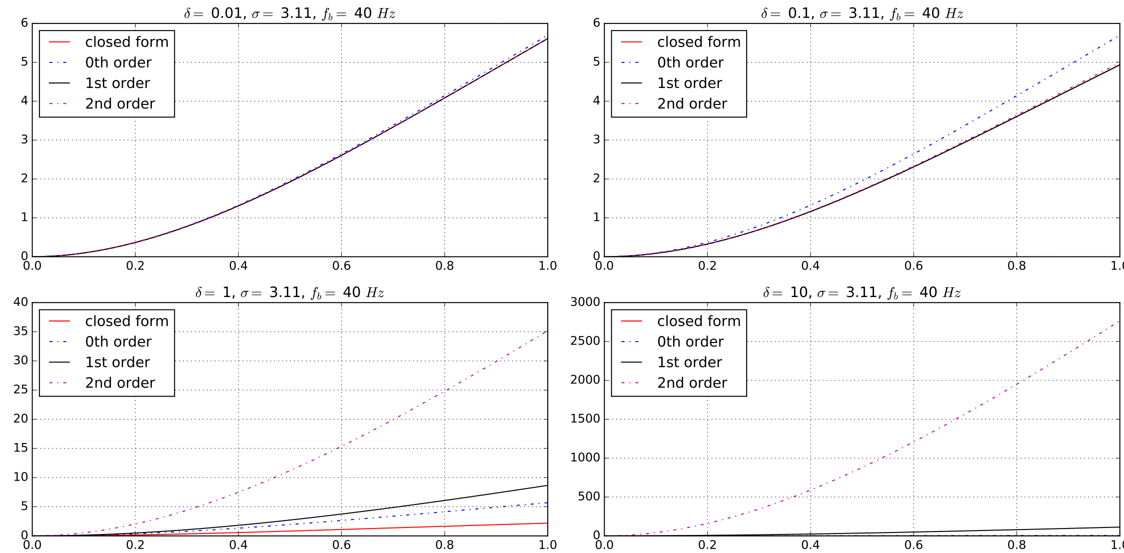

Figure 8: Comparison for the different orders of asymptotic expansion for the dimensionless relative displacement function $u_\delta(z)$.

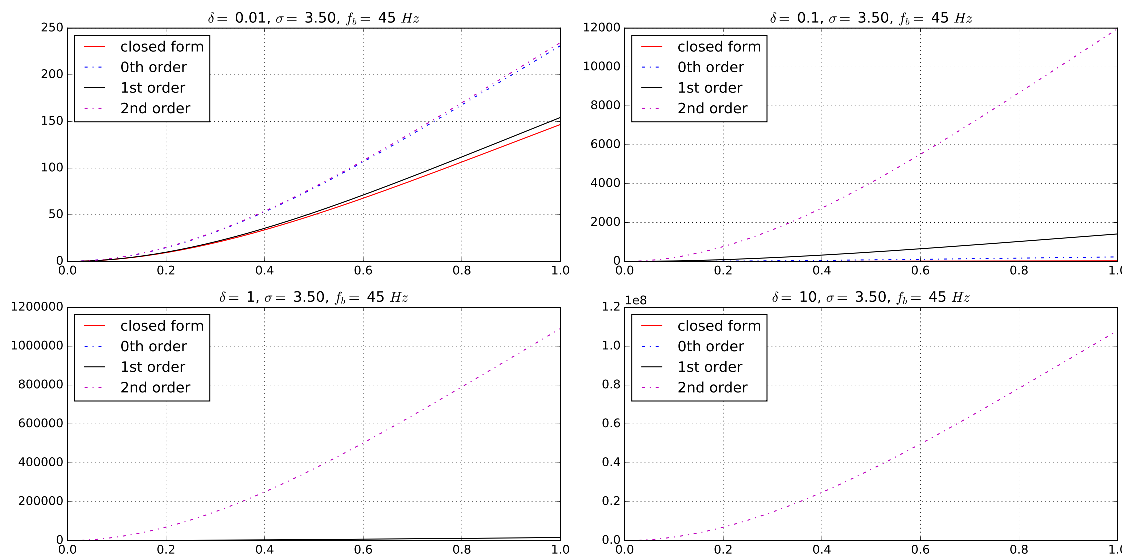

Figure 9: Comparison for the different orders of asymptotic expansion for the dimensionless relative displacement function $u_\delta(z)$.

Theoretically, the first order derivative of the dimensionless relative displacement function $u(z;\delta)$ is

$$u'(z;\delta) = \sigma^{1/2}\left(-A_\delta \sin\sqrt{\sigma}z + B_\delta \cos\sqrt{\sigma}z + C_\delta \sinh\sqrt{\sigma}z + D_\delta \cosh\sqrt{\sigma}z\right). \tag{34}$$

$$\chi_p = u_1'(1) = \frac{\sqrt{\sigma}\left(\sinh\sqrt{\sigma} - \sin\sqrt{\sigma}\right)}{1 + \cos\sqrt{\sigma}\cosh\sqrt{\sigma} + \frac{j\beta\sqrt{\sigma}}{1+j\beta\sigma}\delta\left(\cos\sqrt{\sigma}\sinh\sqrt{\sigma} + \sin\sqrt{\sigma}\cosh\sqrt{\sigma}\right)}. \tag{35}$$

The value of this function at the free end ($z = 1$) is just the output index χ_p according to equation (21). To see the influences of δ and f_b, therefore σ, upon χ_p, we firstly calculate the values of χ_p

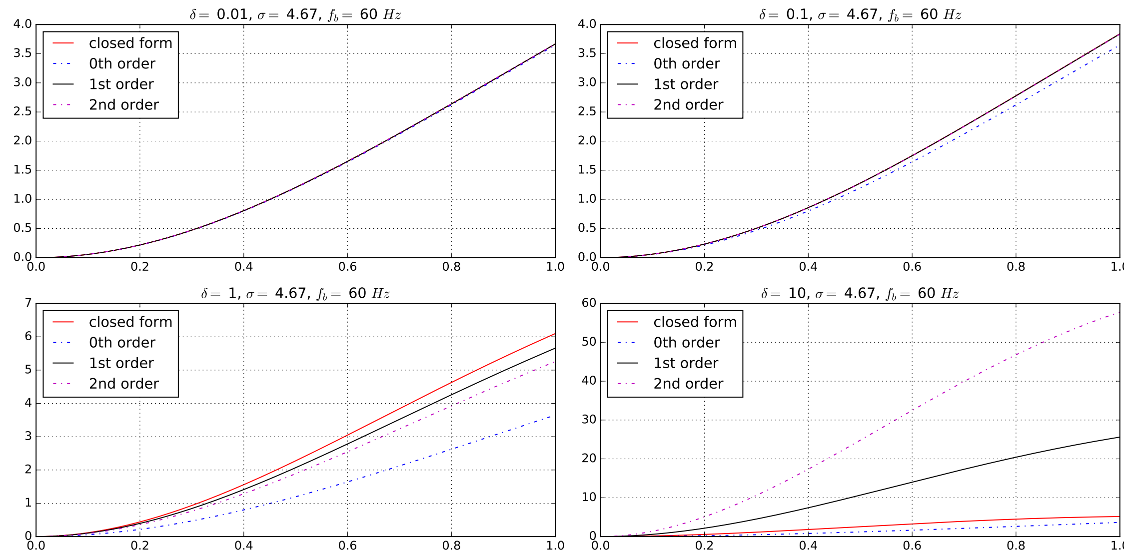

Figure 10: Comparison for the different orders of asymptotic expansion for the dimensionless relative displacement function $u_\delta(z)$.

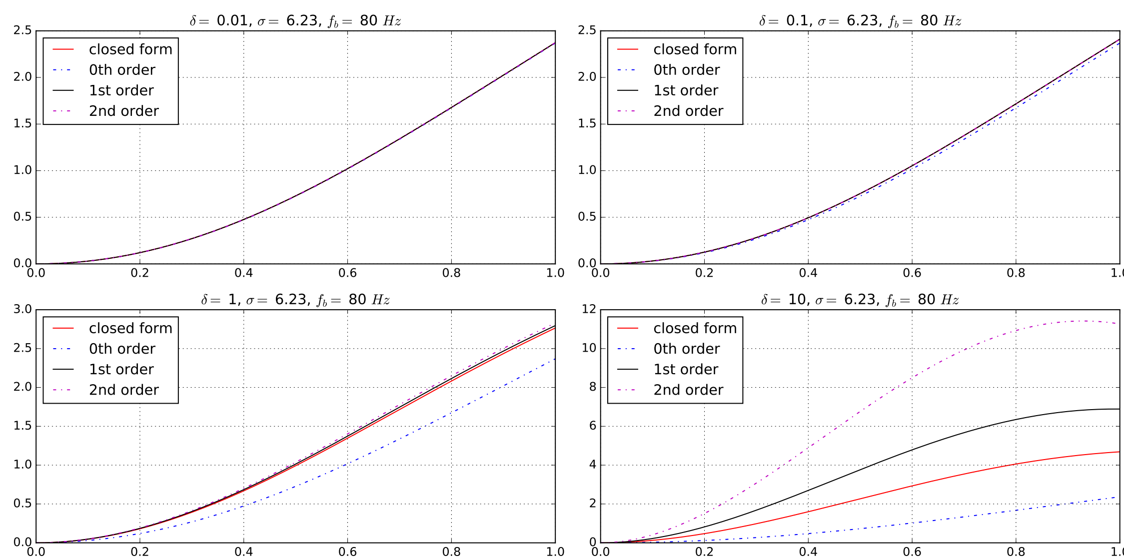

Figure 11: Comparison for the different orders of asymptotic expansion for the dimensionless relative displacement function $u_\delta(z)$.

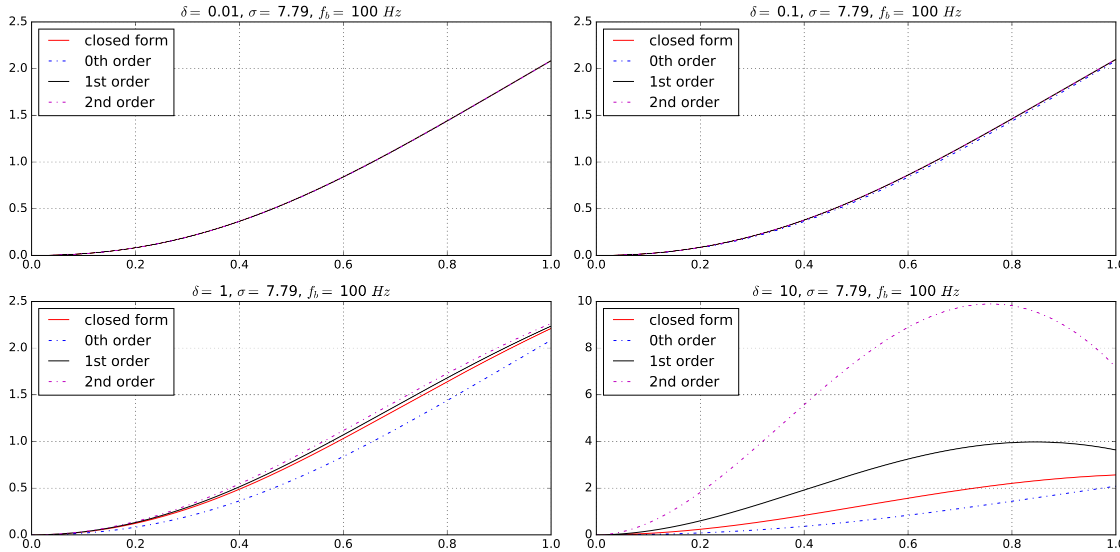

Figure 12: Comparison for the different orders of asymptotic expansion for the dimensionless relative displacement function $u_\delta(z)$.

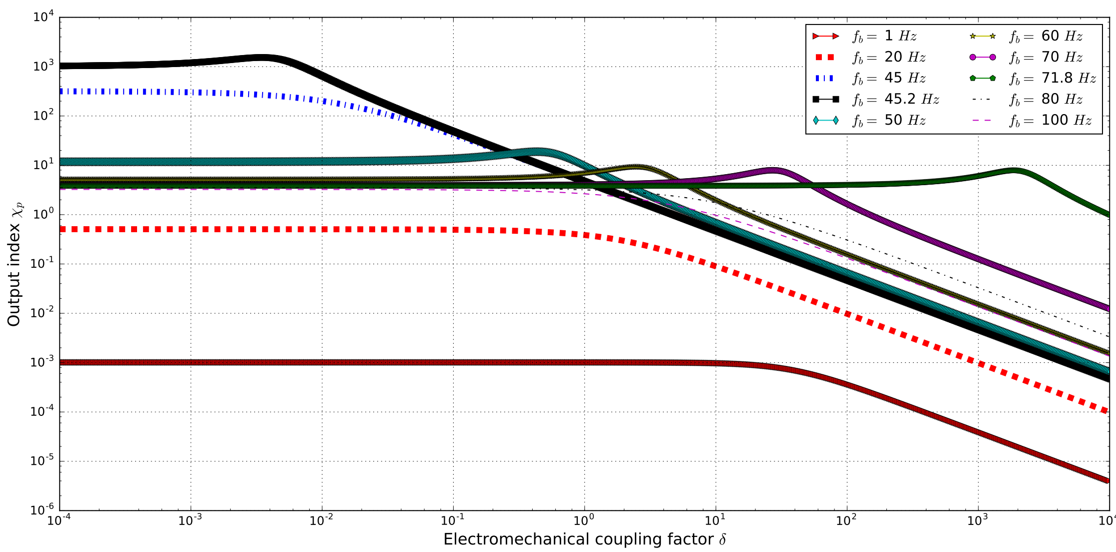

Figure 13: Output index χ_p as a function of electromechanical coupling factor δ at different values of base excitation frequency f_b.

for different values of δ by fixing the value of f_b to be some discrete values. The results are shown in Figure 13.

It is seen that the dependence of χ_p upon δ shows two different modes in the frequency range of $1 - 100\ Hz$. For the frequencies of $45.2\ Hz \leq f_b \leq 71.8\ Hz$, a peak corresponding to a critical value of δ_p is present in the considered range of δ. When δ is smaller than δ_p, the output index χ_p increases along with δ, and when δ is larger than δ_p, the output index χ_p decreases with the increase of δ. On the other hand, for the frequency range of $f_b \leq 45\ Hz$ or $f_b \geq 80\ Hz$, the output index χ_p shows a monotonic decrease with respect to the increase δ.

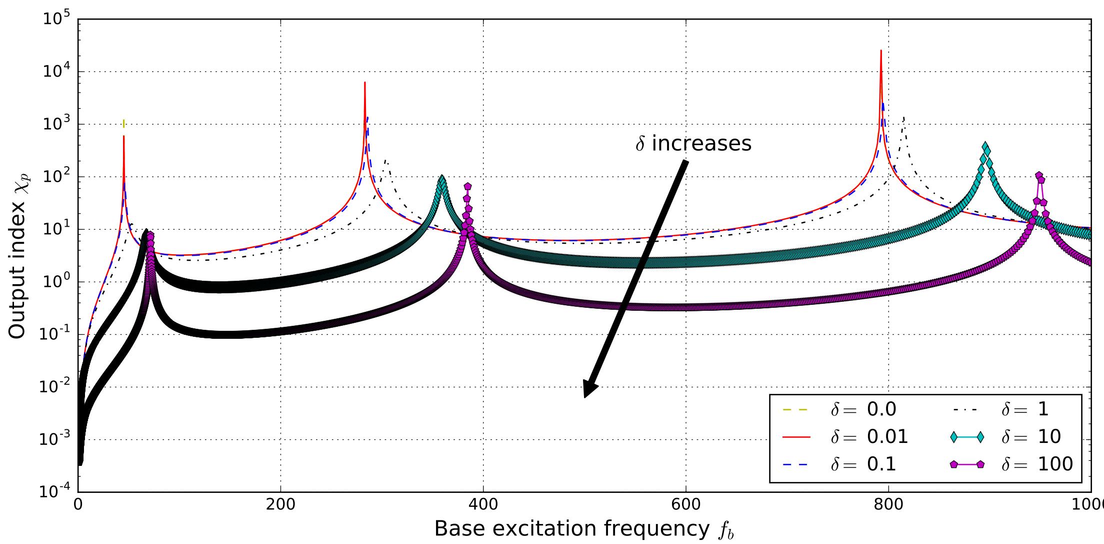

Figure 14: Output index χ_p as a function of base excitation frequency f_b at different values of electromechanical coupling factor δ.

Alternatively, by fixing the values of δ to a discrete set of numbers, we calculate the values of χ_p in relation to different values of f_b. This is very similar to a frequency response of the output index as a function of σ. The results are shown in Figure 14. It is clearly shown that with the increase of electromechanical coupling factor δ, the resonant frequencies to the system increase with the increase of δ. This is clearly shown in the shift to the right of the frequency response curve. Besides, we add in this figure the case where $\delta = 0.0$ as a reference. Simple comparisons show that the discrepancy between the frequency response curves related to the case of $\delta = 0$, $\delta = 0.01$, and $\delta = 0.1$ is small. A direct conclusion is that for relatively small values of electromechanical coupling factor δ, the output index χ_p can be approximated by

$$\chi_p \approx \frac{\sqrt{\sigma}\,(\sinh\sqrt{\sigma} - \sin\sqrt{\sigma})}{1 + \cos\sqrt{\sigma}\cosh\sqrt{\sigma}}. \tag{36}$$

As a result, the output performance measures $\tilde{V}_p$, $\tilde{I}_p$, and $\tilde{P}_p$ can be approximated by

$$\begin{cases} \tilde{V}_p = -\dfrac{j\sigma\beta}{j\sigma\beta+1}\left(\dfrac{\eta_b}{l_p}\right)\left(\dfrac{e_p}{C_p}\right)\chi_p, \\ \quad = -\dfrac{j\sigma\beta}{j\sigma\beta+1}\left(\dfrac{\eta_b}{l_p}\right)\left(\dfrac{e_p}{C_p}\right)\dfrac{\sqrt{\sigma}\,(\sinh\sqrt{\sigma} - \sin\sqrt{\sigma})}{1 + \cos\sqrt{\sigma}\cosh\sqrt{\sigma}}, \\ \tilde{I}_p = \tilde{V}_p/R_l = -\dfrac{j\sigma\beta}{j\sigma\beta+1}\left(\dfrac{\eta_b}{l_p}\right)\left(\dfrac{e_p}{C_pR_l}\right)\chi_p, \\ \quad = -\dfrac{j\sigma\beta}{j\sigma\beta+1}\left(\dfrac{\eta_b}{l_p}\right)\left(\dfrac{e_p}{C_pR_l}\right)\dfrac{\sqrt{\sigma}\,(\sinh\sqrt{\sigma} - \sin\sqrt{\sigma})}{1 + \cos\sqrt{\sigma}\cosh\sqrt{\sigma}}, \\ \tilde{P}_p = \tilde{V}_p^2/R_l = \left(\dfrac{\eta_b}{l_p}\right)^2\left(\dfrac{e_p}{C_p}\right)\left(\dfrac{e_p}{C_pR_l}\right)\left(\dfrac{j\sigma\beta}{j\sigma\beta+1}\right)^2\chi_p^2, \\ \quad = \left(\dfrac{\eta_b}{l_p}\right)^2\left(\dfrac{e_p}{C_p}\right)\left(\dfrac{e_p}{C_pR_l}\right)\left(\dfrac{j\sigma\beta}{j\sigma\beta+1}\right)^2\left(\dfrac{\sqrt{\sigma}\,(\sinh\sqrt{\sigma} - \sin\sqrt{\sigma})}{1 + \cos\sqrt{\sigma}\cosh\sqrt{\sigma}}\right)^2. \end{cases} \tag{37}$$

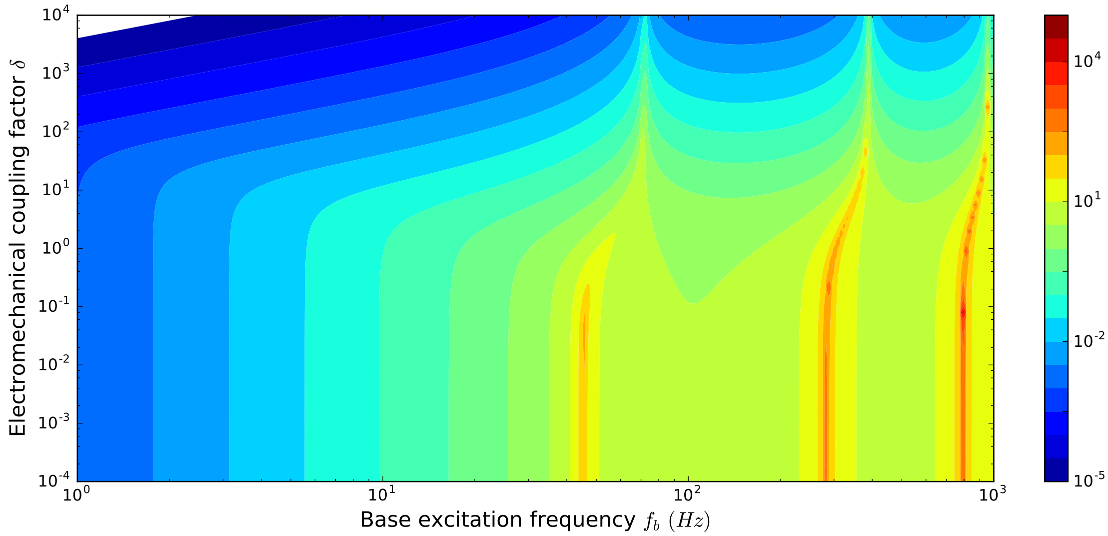

Figure 15: Output index χ_p as a function of base excitation frequency f_b and electromechanical coupling factor δ.

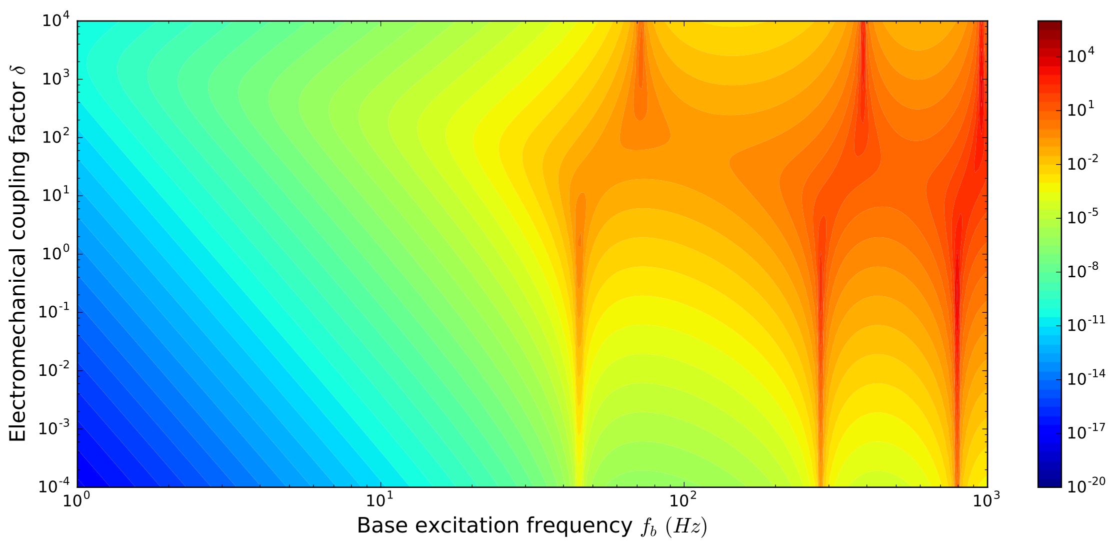

Figure 16: Output voltage $\tilde{V}_p$ as a function of base excitation frequency f_b and electromechanical coupling factor δ.

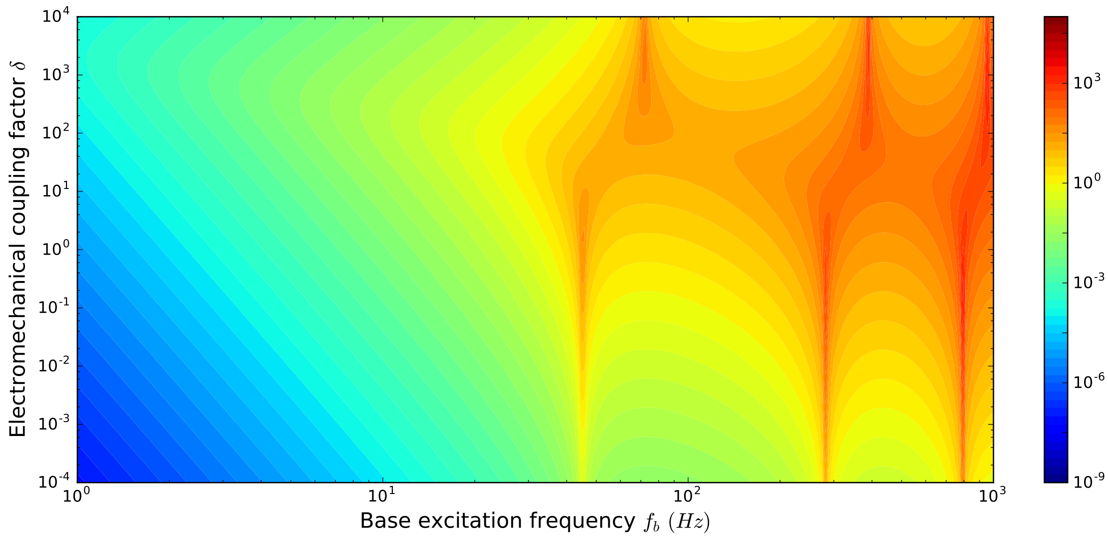

Figure 17: Output voltage $\tilde{P}_p$ as a function of base excitation frequency f_b and electromechanical coupling factor δ.

6 Conclusion

Appendices

The asymptotic expansion of equation (15) can be found using an iterative method. In fact, for higher order expansions ($k \geq 1$), we have the following iterative relation:

$$\begin{cases} A_{k+1} + C_{k+1} = 0, \\ B_{k+1} + D_{k+1} = 0, \\ \left(-A_{k+1}\cos\sqrt{\sigma} - B_{k+1}\sin\sqrt{\sigma} + C_{k+1}\cosh\sqrt{\sigma} + D_{k+1}\sinh\sqrt{\sigma}\right) + \\ \dfrac{j\beta\sqrt{\sigma}}{j\sigma\beta+1}\left(-A_k\sin\sqrt{\sigma} + B_k\cos\sqrt{\sigma} + C_k\sinh\sqrt{\sigma} + D_k\cosh\sqrt{\sigma}\right) = 0, \\ A_{k+1}\sin\sqrt{\sigma} - B_{k+1}\cos\sqrt{\sigma} + C_{k+1}\sinh\sqrt{\sigma} + D_{k+1}\cosh\sqrt{\sigma} = 0, \end{cases} \tag{38}$$

whose solution is expressed by

$$\begin{cases} A_{k+1} = \left(\dfrac{j\beta\sqrt{\sigma}}{1+j\beta\sigma}\right)\left(\dfrac{\cos\sqrt{\sigma}+\cosh\sqrt{\sigma}}{2\cos\sqrt{\sigma}\cosh\sqrt{\sigma}+2}\right)(Q_k), \\ B_{k+1} = \left(\dfrac{j\beta\sqrt{\sigma}}{1+j\beta\sigma}\right)\left(\dfrac{-\sinh\sqrt{\sigma}+\sin\sqrt{\sigma}}{2\cos\sqrt{\sigma}\cosh\sqrt{\sigma}+2}\right)(Q_k), \\ C_{k+1} = \left(\dfrac{j\beta\sqrt{\sigma}}{1+j\beta\sigma}\right)\left(-\dfrac{\cos\sqrt{\sigma}+\cosh\sqrt{\sigma}}{2\cos\sqrt{\sigma}\cosh\sqrt{\sigma}+2}\right)(Q_k), \\ D_{k+1} = \left(\dfrac{j\beta\sqrt{\sigma}}{1+j\beta\sigma}\right)\left(\dfrac{-\sin\sqrt{\sigma}+\sinh\sqrt{\sigma}}{2\cos\sqrt{\sigma}\cosh\sqrt{\sigma}+2}\right)(Q_k), \end{cases} \tag{39}$$

in which

$$Q_k = -A_k\sin\sqrt{\sigma} + B_k\cos\sqrt{\sigma} + C_k\sinh\sqrt{\sigma} + D_k\cosh\sqrt{\sigma}. \tag{40}$$

In terms of Q_k ($k \geq 0$), we have the following iterative relation

$$Q_{k+1} = -\left(\frac{\sin\sqrt{\sigma}\cosh\sqrt{\sigma}+\cos\sqrt{\sigma}\sinh\sqrt{\sigma}}{\cos\sqrt{\sigma}\cosh\sqrt{\sigma}+1}\right)\left(\frac{j\beta\sqrt{\sigma}}{1+j\beta\sigma}\right)Q_k, \tag{41}$$

and the initial two values Q_0 and Q_1:

$$\begin{cases} Q_0 = \dfrac{\sinh\sqrt{\sigma}-\sin\sqrt{\sigma}}{\cos\sqrt{\sigma}\cosh\sqrt{\sigma}+1}, \\ Q_1 = \dfrac{j\beta\sqrt{\sigma}}{1+j\beta\sigma}\left(\dfrac{\sin\sqrt{\sigma}-\sinh\sqrt{\sigma}}{\cos\sqrt{\sigma}\cosh\sqrt{\sigma}+1}\right)\left(\dfrac{\cos\sqrt{\sigma}\sinh\sqrt{\sigma}+\sin\sqrt{\sigma}\cosh\sqrt{\sigma}}{\cos\sqrt{\sigma}\cosh\sqrt{\sigma}+1}\right). \end{cases} \tag{42}$$

Hence it is shown that for $k \geq 0$,

$$Q_k = \left[-\left(\frac{j\beta\sqrt{\sigma}}{1+j\beta\sigma} \right) \left(\frac{\sin\sqrt{\sigma}\cosh\sqrt{\sigma} + \cos\sqrt{\sigma}\sinh\sqrt{\sigma}}{\cos\sqrt{\sigma}\cosh\sqrt{\sigma}+1} \right) \right]^k \left(\frac{\sinh\sqrt{\sigma} - \sin\sqrt{\sigma}}{\cos\sqrt{\sigma}\cosh\sqrt{\sigma}+1} \right). \tag{43}$$

As a result, we obtain that for $k \geq 1$,

$$\begin{cases} A_k = \left(\frac{j\beta\sqrt{\sigma}}{1+j\beta\sigma} \right)^k \left(\frac{-\sin\sqrt{\sigma}\cosh\sqrt{\sigma} - \cos\sqrt{\sigma}\sinh\sqrt{\sigma}}{\cos\sqrt{\sigma}\cosh\sqrt{\sigma}+1} \right)^{k-1} \left(\frac{\sinh\sqrt{\sigma} - \sin\sqrt{\sigma}}{\cos\sqrt{\sigma}\cosh\sqrt{\sigma}+1} \right) \left(\frac{\cos\sqrt{\sigma} + \cosh\sqrt{\sigma}}{2\cos\sqrt{\sigma}\cosh\sqrt{\sigma}+2} \right), \\ B_k = \left(\frac{j\beta\sqrt{\sigma}}{1+j\beta\sigma} \right)^k \left(\frac{-\sin\sqrt{\sigma}\cosh\sqrt{\sigma} - \cos\sqrt{\sigma}\sinh\sqrt{\sigma}}{\cos\sqrt{\sigma}\cosh\sqrt{\sigma}+1} \right)^{k-1} \left(\frac{\sinh\sqrt{\sigma} - \sin\sqrt{\sigma}}{\cos\sqrt{\sigma}\cosh\sqrt{\sigma}+1} \right) \left(\frac{-\sinh\sqrt{\sigma} + \sin\sqrt{\sigma}}{2\cos\sqrt{\sigma}\cosh\sqrt{\sigma}+2} \right), \\ C_k = \left(\frac{j\beta\sqrt{\sigma}}{1+j\beta\sigma} \right)^k \left(\frac{-\sin\sqrt{\sigma}\cosh\sqrt{\sigma} - \cos\sqrt{\sigma}\sinh\sqrt{\sigma}}{\cos\sqrt{\sigma}\cosh\sqrt{\sigma}+1} \right)^{k-1} \left(\frac{\sinh\sqrt{\sigma} - \sin\sqrt{\sigma}}{\cos\sqrt{\sigma}\cosh\sqrt{\sigma}+1} \right) \left(\frac{-\cos\sqrt{\sigma} - \cosh\sqrt{\sigma}}{2\cos\sqrt{\sigma}\cosh\sqrt{\sigma}+2} \right), \\ D_k = \left(\frac{j\beta\sqrt{\sigma}}{1+j\beta\sigma} \right)^k \left(\frac{-\sin\sqrt{\sigma}\cosh\sqrt{\sigma} - \cos\sqrt{\sigma}\sinh\sqrt{\sigma}}{\cos\sqrt{\sigma}\cosh\sqrt{\sigma}+1} \right)^{k-1} \left(\frac{\sinh\sqrt{\sigma} - \sin\sqrt{\sigma}}{\cos\sqrt{\sigma}\cosh\sqrt{\sigma}+1} \right) \left(\frac{-\sin\sqrt{\sigma} + \sinh\sqrt{\sigma}}{2\cos\sqrt{\sigma}\cosh\sqrt{\sigma}+2} \right). \end{cases}$$

Acknowledgements

References

[1] Beeby SP, Tudor MJ, White N. Energy harvesting vibration sources for microsystems applications. Measurement science and technology. 2006;17(12):R175.

[2] Anton SR, Sodano HA. A review of power harvesting using piezoelectric materials (2003–2006). Smart materials and Structures. 2007;16(3):R1.

[3] Zhou M, Al-Furjan MSH, Zou J, Liu W. A review on heat and mechanical energy harvesting from human–Principles, prototypes and perspectives. Renewable and Sustainable Energy Reviews. 2018;82:3582–3609.

[4] Safaei M, Sodano HA, Anton SR. A review of energy harvesting using piezoelectric materials: state-of-the-art a decade later (2008–2018). Smart Materials and Structures. 2019;28(11):113001.

[5] Roundy S, Wright PK, Rabaey J. A study of low level vibrations as a power source for wireless sensor nodes. Computer communications. 2003;26(11):1131–1144.

[6] Dutoit NE, Wardle BL, Kim SG. Design considerations for MEMS-scale piezoelectric mechanical vibration energy harvesters. Integrated ferroelectrics. 2005;71(1):121–160.

[7] Stephen NG. On energy harvesting from ambient vibration. Journal of sound and vibration. 2006;293(1-2):409–425.

[8] Cottone F, Vocca H, Gammaitoni L. Nonlinear energy harvesting. Physical Review Letters. 2009;102(8):080601.

[9] Erturk A, Inman DJ. On mechanical modeling of cantilevered piezoelectric vibration energy harvesters. Journal of intelligent material systems and structures. 2008;19(11):1311–1325.

[10] Crandall SH. Dynamics of mechanical and electromechanical systems. McGraw-Hill; 1968.

[11] Hagood NW, Chung WH, Von Flotow A. Modelling of piezoelectric actuator dynamics for active structural control. Journal of intelligent material systems and structures. 1990;1(3):327–354.

[12] Sodano HA, Park G, Inman D. Estimation of electric charge output for piezoelectric energy harvesting. Strain. 2004;40(2):49–58.

[13] Lu F, Lee H, Lim S. Modeling and analysis of micro piezoelectric power generators for micro-electromechanical-systems applications. Smart Materials and Structures. 2003;13(1):57.

[14] Chen SN, Wang GJ, Chien MC. Analytical modeling of piezoelectric vibration-induced micro power generator. Mechatronics. 2006;16(7):379–387.

[15] Ajitsaria J, Choe SY, Shen D, Kim D. Modeling and analysis of a bimorph piezoelectric cantilever beam for voltage generation. Smart Materials and Structures. 2007;16(2):447.

[16] Kreyszig E. Introductory functional analysis with applications. vol. 1. wiley New York; 1978.

[17] Erturk A, Inman DJ. A distributed parameter electromechanical model for cantilevered piezoelectric energy harvesters. Journal of vibration and acoustics. 2008;130(4):041002.

[18] Erturk A, Inman DJ. An experimentally validated bimorph cantilever model for piezoelectric energy harvesting from base excitations. Smart materials and structures. 2009;18(2):025009.

[19] Erturk A, Tarazaga PA, Farmer JR, Inman DJ. Effect of strain nodes and electrode configuration on piezoelectric energy harvesting from cantilevered beams. Journal of Vibration and Acoustics. 2009;131(1):011010.

[20] Shu Y, Lien I. Analysis of power output for piezoelectric energy harvesting systems. Smart materials and structures. 2006;15(6):1499.

[21] Shu Y, Lien I, Wu W. An improved analysis of the SSHI interface in piezoelectric energy harvesting. Smart Materials and Structures. 2007;16(6):2253.

[22] Qiu J, Jiang H, Ji H, Zhu K. Comparison between four piezoelectric energy harvesting circuits. Frontiers of Mechanical Engineering in China. 2009;4(2):153–159.

[23] Weaver Jr W, Timoshenko SP, Young DH. Vibration problems in engineering. John Wiley & Sons; 1990.